Supplement of Atmos. Chem. Phys., 22, 8117–8136, 2022
https://doi.org/10.5194/acp-22-8117-2022-supplement

Atmospheric Chemistry and Physics Open Access

Supplement of

Measurement report: Distinct size dependence and diurnal variation in organic aerosol hygroscopicity, volatility, and cloud condensation nuclei activity at a rural site in the Pearl River Delta (PRD) region, China

Mingfu Cai et al.

Correspondence to: Shan Huang (shanhuang_eci@jnu.edu.cn) and Li Liu (liul@gd121.cn)

Section S1. Supersaturation calibration of the CCNc

Before and after the measurement, the CCNc was calibrated with ammonium sulfate ($(NH_4)_2SO_4$) particles. The critical supersaturation (Sc) was calculated by using Köhler theory:

$$Sc = exp\left[\left(\frac{4A^3}{27B}\right)^{1/2}\right], A = \frac{4\sigma_{s/a}M_w}{RT\rho_w}, B = \frac{6i_s n_s M_w}{\pi\rho_w} \quad \text{(S1)}$$

where $\sigma_{s/a}$ is the surface tension of the solution/air interface and is assumed to be pure water (0.0728 N m^{-1} at 298.15 K) for simplicity, M_w is the molecular weight of water (0.018 kg mol^{-1}), R is the universal gas constant (8.314 J mol^{-1} K^{-1}), T is the thermodynamic temperature in Kelvin (298.15 K), ρ_w is the density of water (about 997.04 kg m^{-3} at 298.15 K), i_s is the van't Hoff factor and is assumed to be 2.5, n_s is the molality of $(NH_4)_2SO_4$, $n_s = \frac{\pi\rho_s D_{50}^3}{6M_s}$, D_{50} is the critical diameter, ρ_s is the density of ammonium sulfate (1769 kg m^{-3}), and M_s is the mole mass of ammonium sulfate (0.132 kg mol^{-1}).

Section S2. Estimation of the uncertainty caused by the decomposition

During the heating process, ammonium sulfate ($(NH_4)_2SO_4$) would decompose to ammonium bisulfate (NH_4HSO_4) or triammonium hydrogen sulfate ($(NH_4)_3H(SO_4)_2$, and ammonia (NH_3). Meanwhile, extremely low volatile OA (ELVOA) would decompose into semi-volatile or low-volatile OA. This could lead to uncertainty in the simulation. To estimate the uncertainty, we simulate the campaign average data based on the following assumptions:

Case 1. All $(NH_4)_2SO_4$ would decompose to $(NH_4)_3H(SO_4)_2$ at 150°C and then sublimation, while the decomposition of organics is ignored.

Case 2. All ELVOA would decompose to SVOA at 100°C, while the decomposition of ammonium sulfate is ignored.

Case 3. All $(NH_4)_2SO_4$ would decompose to $(NH_4)_3H(SO_4)_2$ and sublimation at 150°C, and all of EVLOA would decompose to SVOA at 100°C.

The results show that the decomposition of $(NH_4)_2SO_4$ plays a minor role in the simulation if the decomposition of organics was ignored (Case 1, Fig. S6). It is probably owing to the fact that $(NH_4)_2SO_4$ starts to volatilize at about 100°C and completely sublimate at about 200°C (Hong et al., 2017). The decomposition of organics would significantly increase the fraction of SVOA (Case 2 and 3) by about 0.15-0.54. However, the SSR increases from 0.0216 in the standard simulation (ignore decomposition) to 0.5277 and 0.6626 in the case 2 and 3, respectively, suggesting that the model fails to reproduce the MFR based on the adopted parameters (ΔH_vap=80 kJ mol-1 and α=0.09). Thus, the results in case 2 and 3 are highly uncertain. In short summary, the decomposition of $(NH_4)_2SO_4$ would lead to a minor uncertainty in the simulation, while the decomposition of organic matter would significantly affect the model results by increasing the fraction of SVOA, for which the exact effects were still unclear. Further investigations are needed to better understand the decomposition of particles during the heating processes.

Section S3. The impact of aerosol mixing state on the N_{CCN} prediction

The N_{CCN} prediction is affected by the assumed particle mixing state (Wang et al., 2010). We estimated the impact of the mixing state assumption on the N_{CCN} prediction by comparing the predicted N_{CCN} based on AMS and HTDMA measurements. For the prediction based on AMS measurement, the particles were assumed to be internally mixed. In the latter approach, the mixing state was considered. The hygroscopicity parameter $\kappa_{critical}(Dp, SS)$ was defined as the point at which all particles could be activated at a specific diameter (Dp) and a specific SS. We calculated the $\kappa_{critical}(Dp, SS)$ using eq. (4) for a measured diameter (Dp) and a known SS. Particles with a κ value higher than the $\kappa_{critical}(Dp, SS)$ were activated. The activation ratio ($AR_{HTDMA}(Dp, SS)$) for a known diameter and SS was obtained by integrating the κ-PDF for $\kappa > \kappa_{critical}(Dp, SS)$. Hence the predicted activation curve $AR_p(Dp, SS)$ was determined by fitting the $AR_{HTDMA}(Dp, SS)$ using eq. (6). Thus, the N_{CCN} can be calculated:

$$N_{CCN,p}(SS) = \int_0^\infty AR_p(Dp_i, SS) n_i d\log Dp_i \quad \text{(S2)}$$

the detail of this approach could be found in Cai et al. (2018).

In general, the combination of the internal mixing assumption and fixed κ_{OA} scheme would lead to an overestimation of N_{CCN} (14%-23%, Fig. S11). Noting that adopting a fixed κ_{OA} value could also overpredict N_{CCN} (especially at high SS), which has been discussed in the text (section 3.4). This bias could be corrected by adopting SR κ_{OA} scheme, which showed that the N_{CCN} was overestimated by about 6%-10% (Fig. S11). Hence, we concluded that assuming the particle to be an internal mixture could lead to an overestimation of N_{CCN} by about 6%-10%.

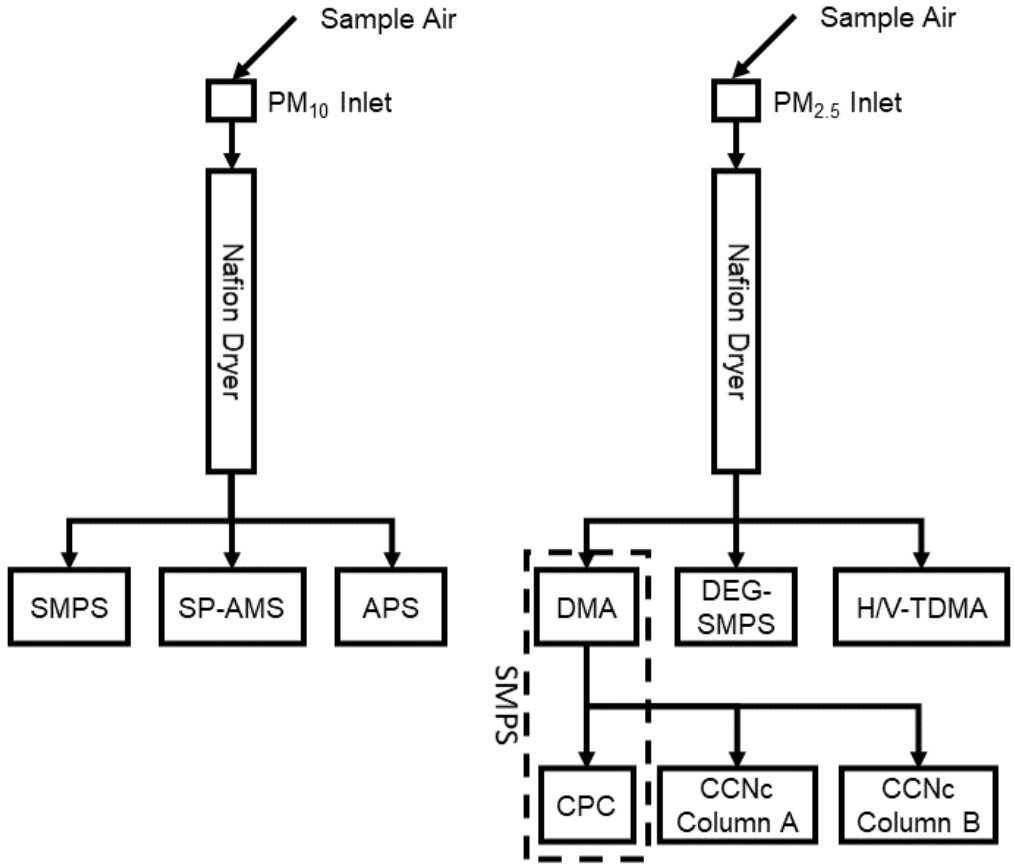

Figure S1. Schematic diagram of the experimental setup

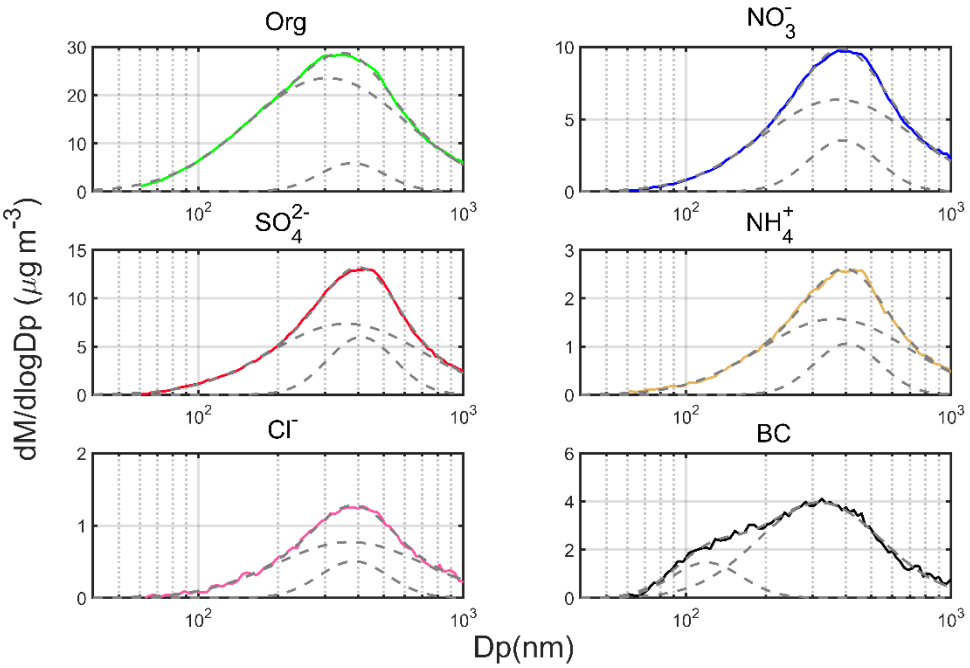

Figure S2. The average mass distribution of each species measured by the AMS, along with bimodal lognormal fitted modes (grey dash line).

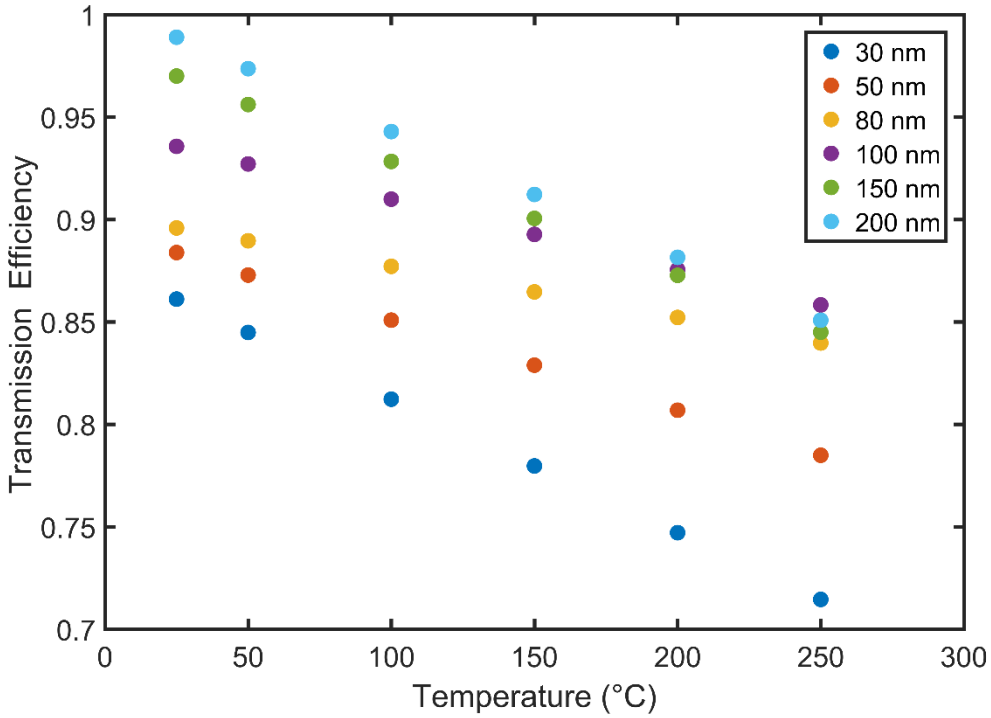

Figure S3. The transmission efficiency (η) of NaCl between DMA_1 and DMA_2 at different sizes and temperatures.

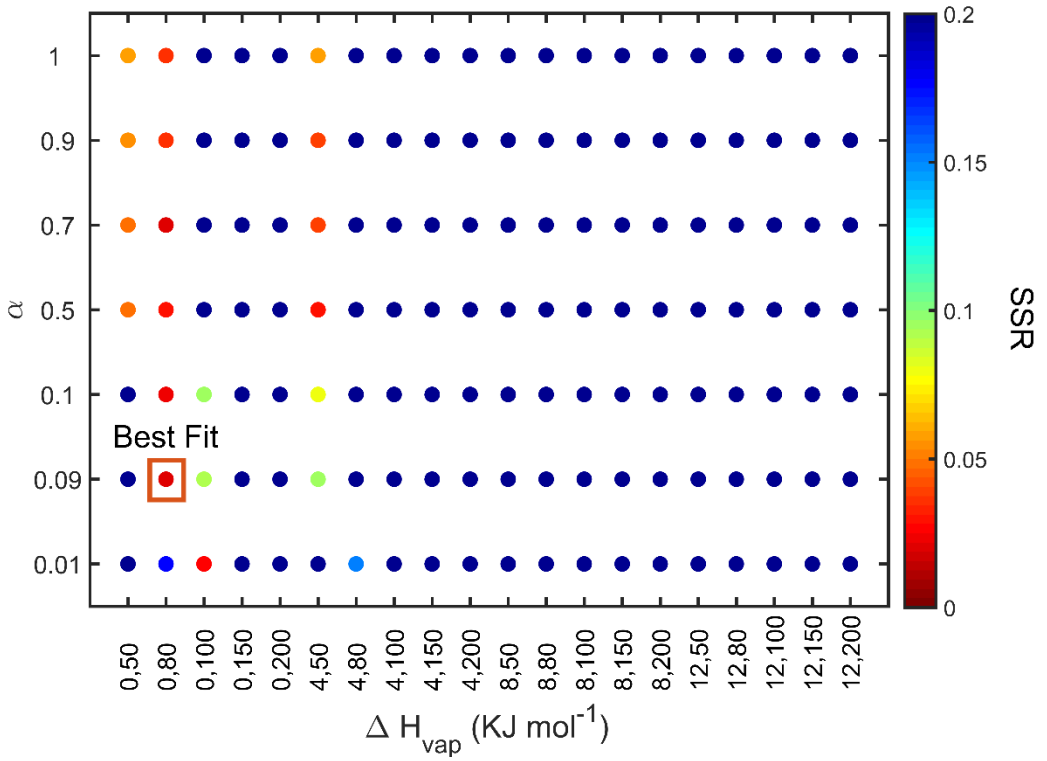

Figure S4. SSR values of different fitness of the campaign averaged MFR. The color code represents the value of SSR. The distribution of each species is solved based on different combinations of ΔH_{vap} of OA and α. The ΔH_{vap} is assumed to be as a function of $C_i^*(T_{ref})$, $\Delta H_{vap} = -a \cdot log_{10} C_i^*(T_{ref}) + b$, e.g., "0, 50" on the x axis suggests a=0 and b=50. A lower SSR suggests a better fit. The orange square represents the best fitting results.

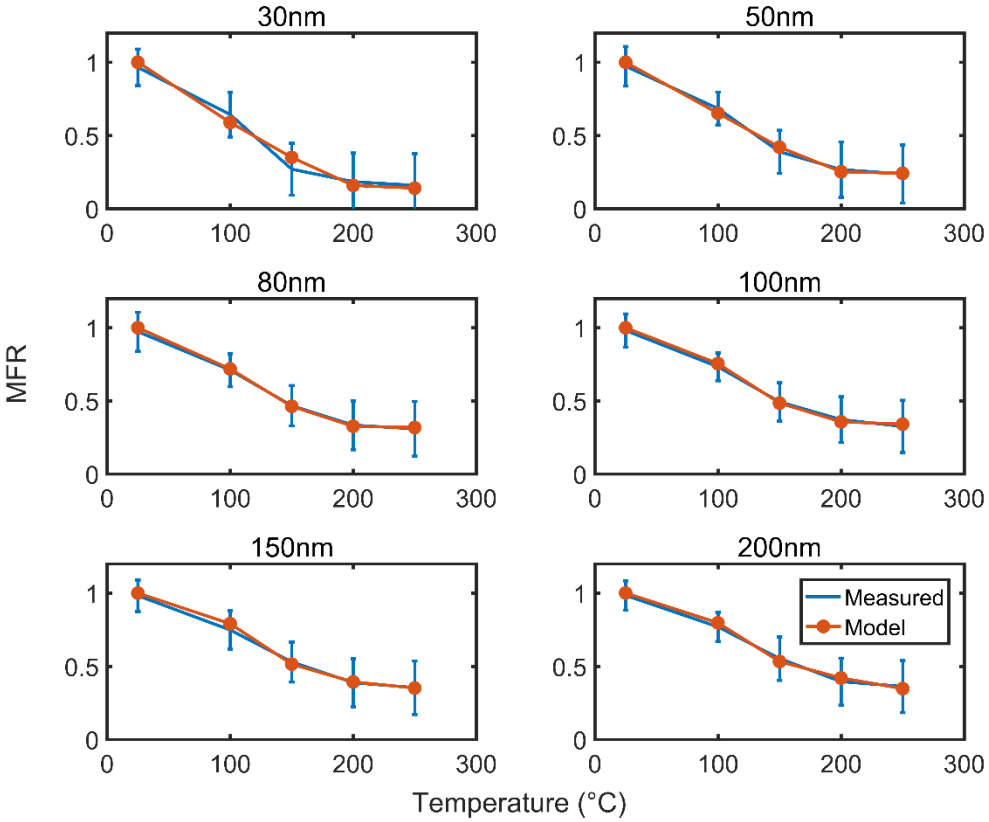

Figure S5. Measured (blue lines) and modeled (red lines) campaign average MFRs at six measured diameters (30, 50, 80, 100, 150, and 200 nm). The error bar of measured MFRs represents $\pm$ 1 standard deviation. ΔH_{vap}=80 kJ mol^{-1} and α=0.09 are adopted in the simulation.

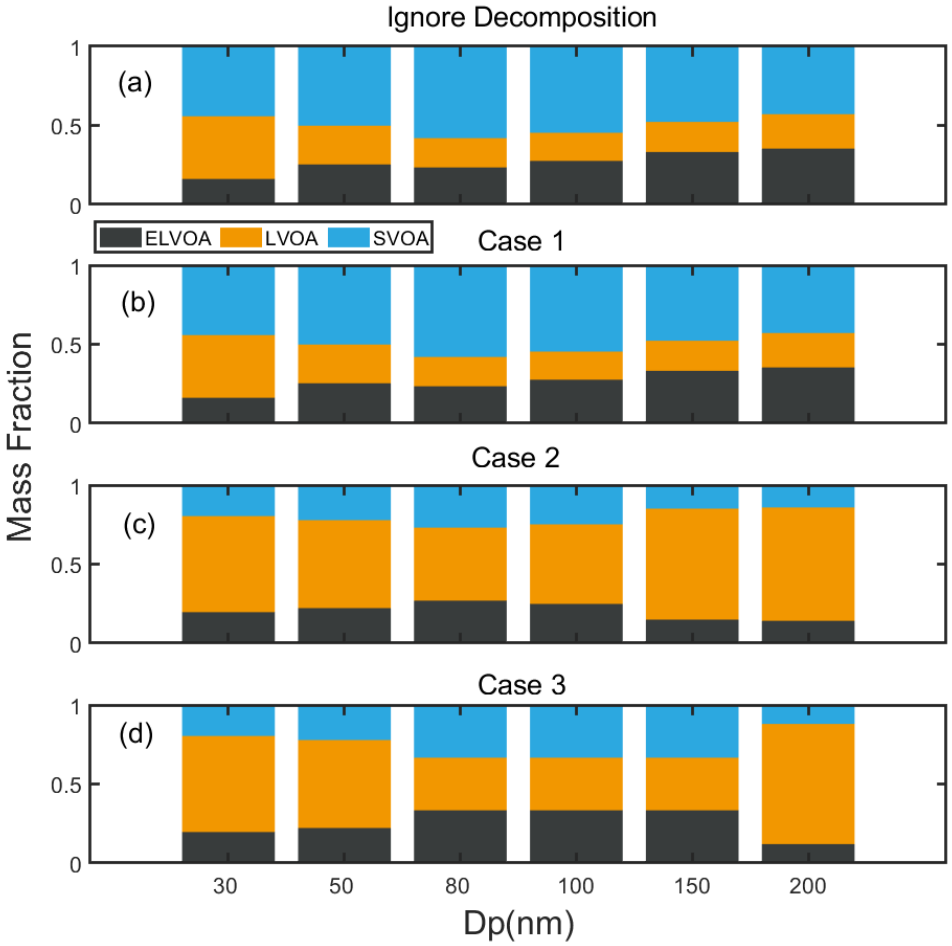

Figure S6. The mass fraction distribution of SVOA, LVOA, and ELVOA of the campaign averaged MFR based on different assumptions.

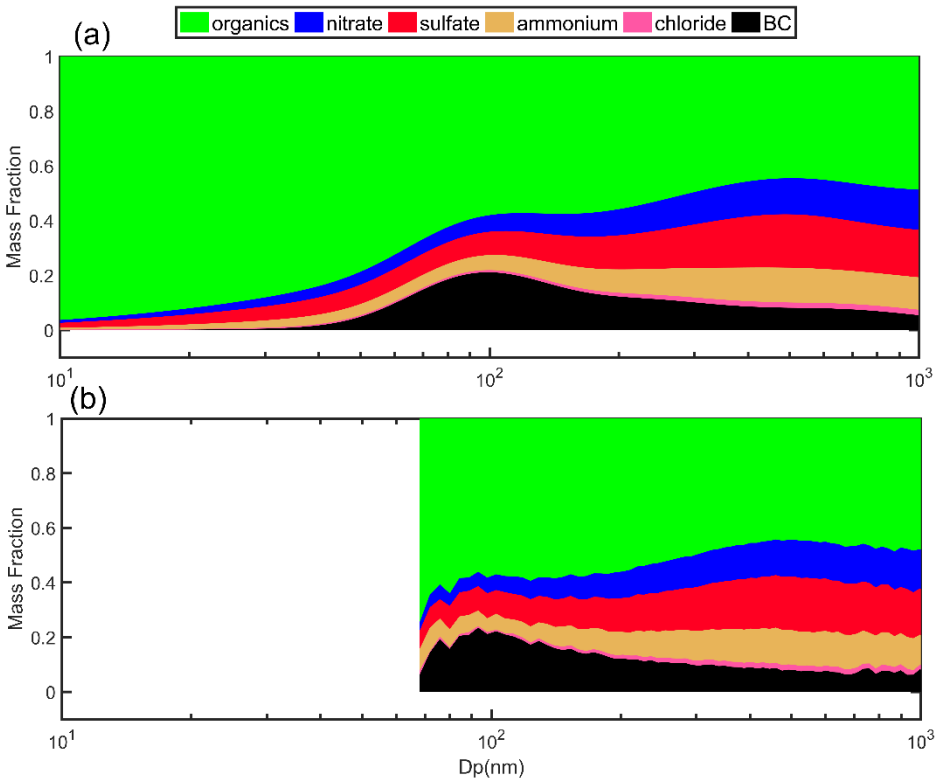

Figure S7. The average mass fraction of the size-resolved composition based on the lognormal fit (a) and measurement (b).

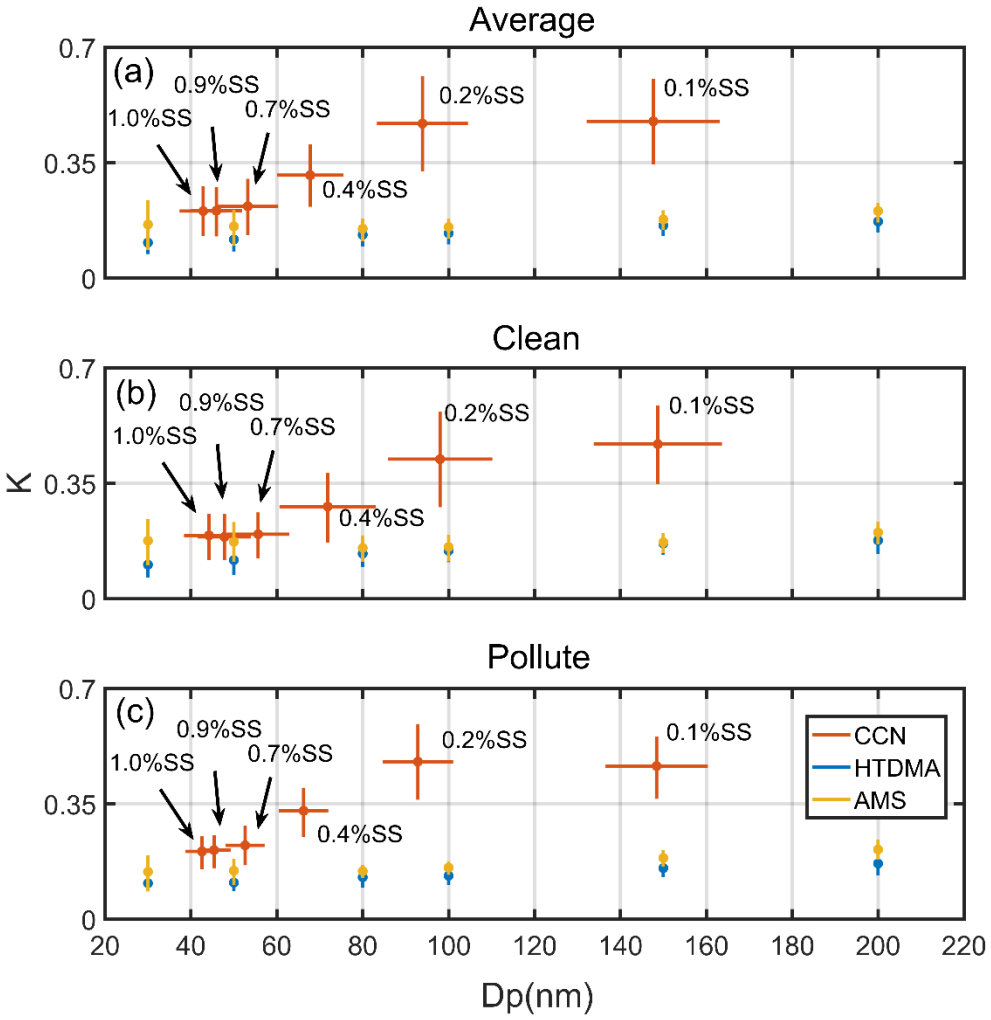

Figure S8. The mean and standard deviation values of κ_{CCN}, κ_{HTDMA}, and κ_{AMS} during the campaign (a), clean (b) and pollute periods (c). The κ values were pointed against their corresponding mean D_{50} (κ_{CCN}) or selected diameter (κ_{HTDMA} and κ_{AMS}). The dots represent the mean values, and the bars represent the one standard deviation. The relative clean and polluted periods were classified by the mass concentration of $PM_{2.5}$ (< 30 μg m^{-3} and > 60 μg m^{-3}, respectively).

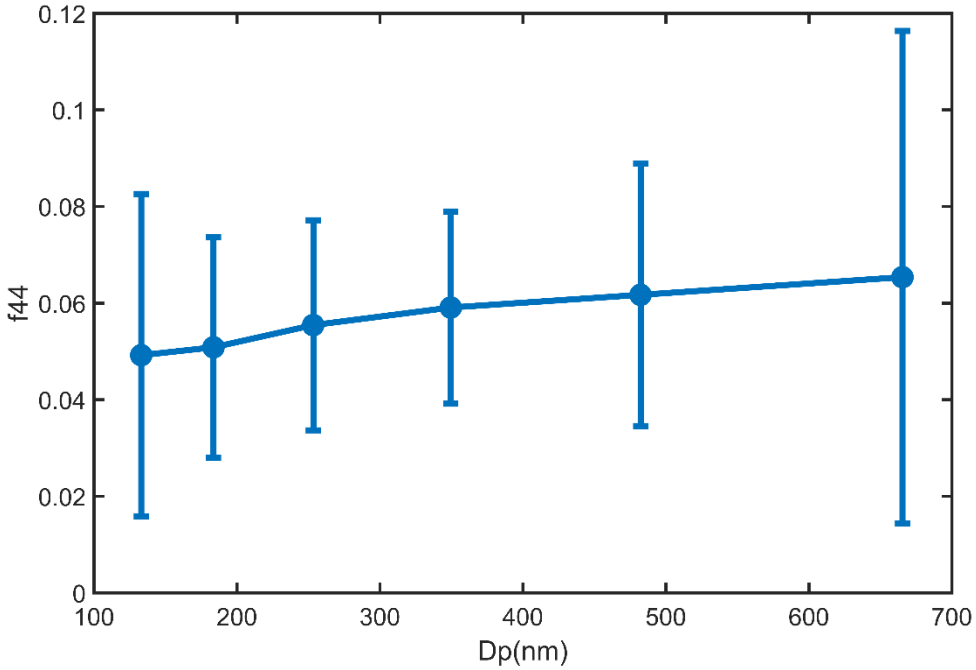

Figure S9. The campaign average size-resolved f44 with the upper and lower error bars.

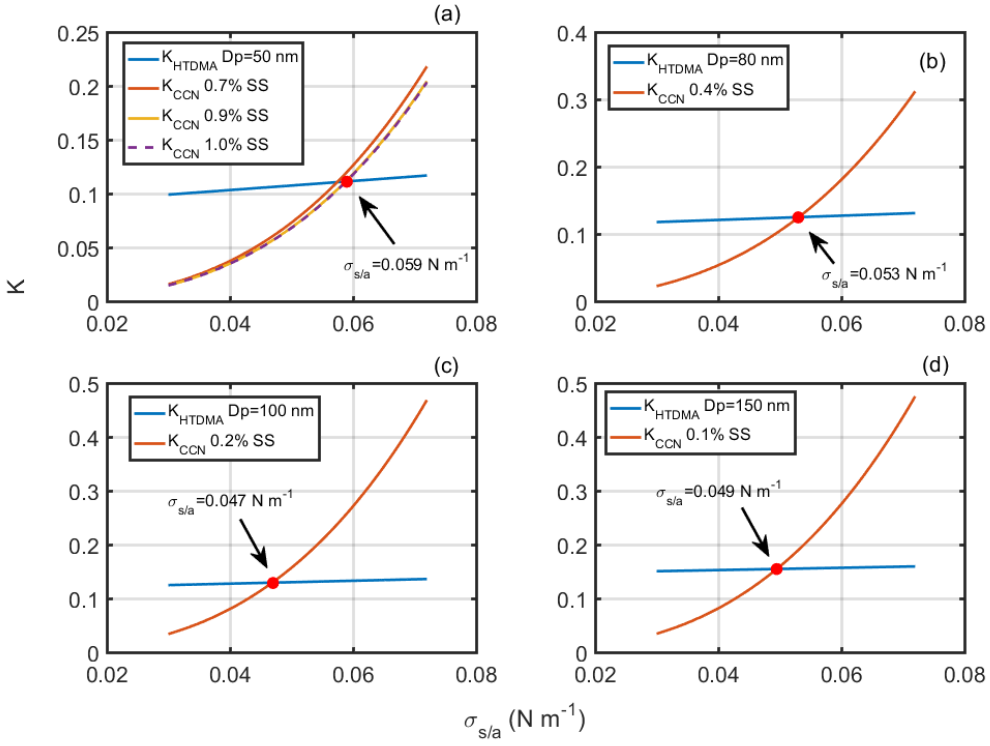

Figure S10. κ_{CCN} and κ_{HTDMA} at different assumed $\sigma_{s/a}$. κ_{HTDMA} at 50, 80, 100 and 150 nm is adopted to compared with κ_{CCN} at 0.7%, 0.9%, and 1.0% SS, 0.4% SS, 0.2% SS, and 0.1% SS, respectively. Red dot represents the intersection point of κ_{CCN} and κ_{HTDMA}.

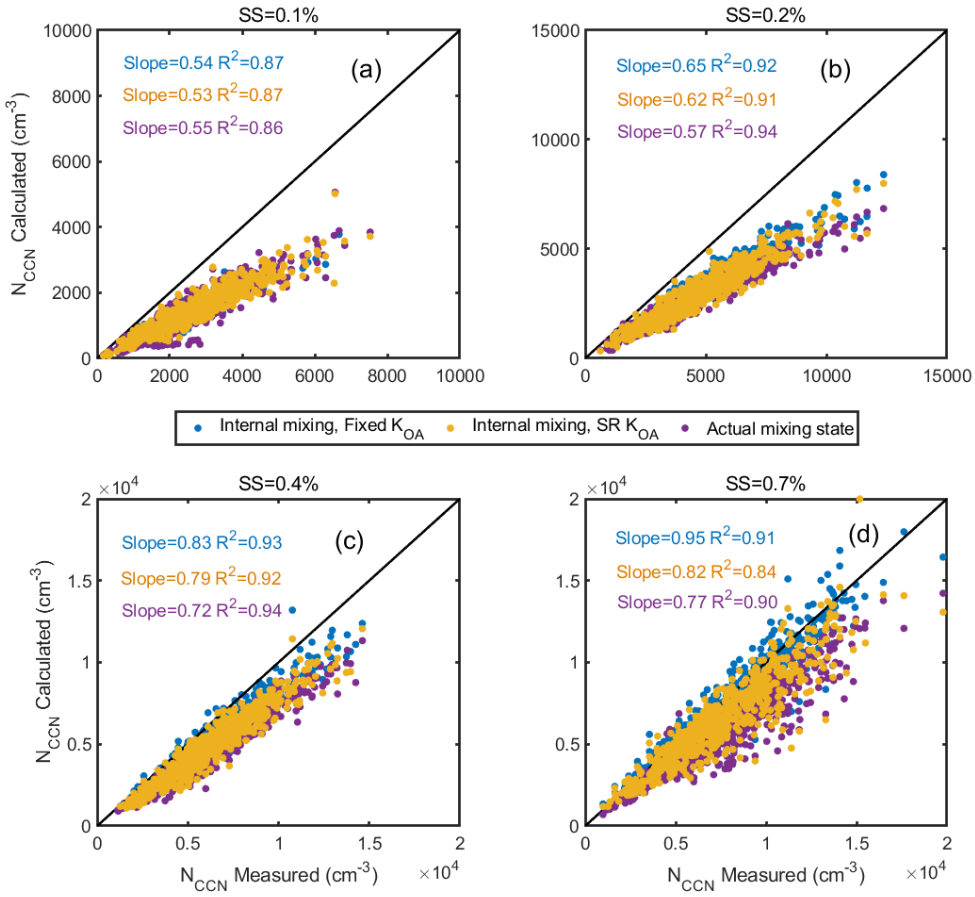

Figure S11. The predicted and measured N_{CCN} at 0.1%, 0.2%, 0.4%, and 0.7% SS based on internal mixing assumption (blue and yellow dots) and actual mixing state (purple dots). The fixed κ_{OA} scheme (blue dots) and SR κ_{OA} scheme (yellow dots) were adopted in the prediction based on the internal mixing assumption.

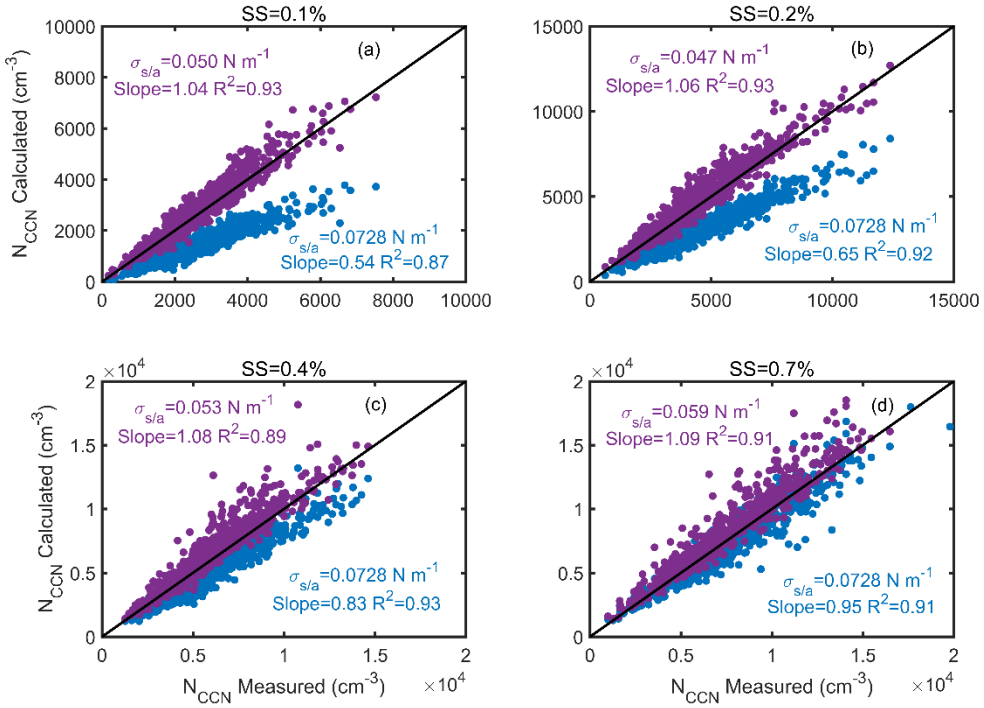

Figure S12. The measured and predicted N_{CCN} at 0.1%, 0.2%, 0.4%, and 0.7% SS based on the $\sigma_{s/a}$ value (0.0728 N m^{-1}) for pure water (bule dots) and reduced $\sigma_{s/a}$ values (purple dots). The reduced $\sigma_{s/a}$ values were set to be 0.049 N m^{-1} at 0.1% SS, 0.047 N m^{-1} at 0.2% SS, 0.053 N m^{-1} at 0.4% SS, and 0.059 N m^{-1} at 0.7% SS, respectively. The N_{CCN} at four SS was predicted based on fixed κ_{OA} scheme.

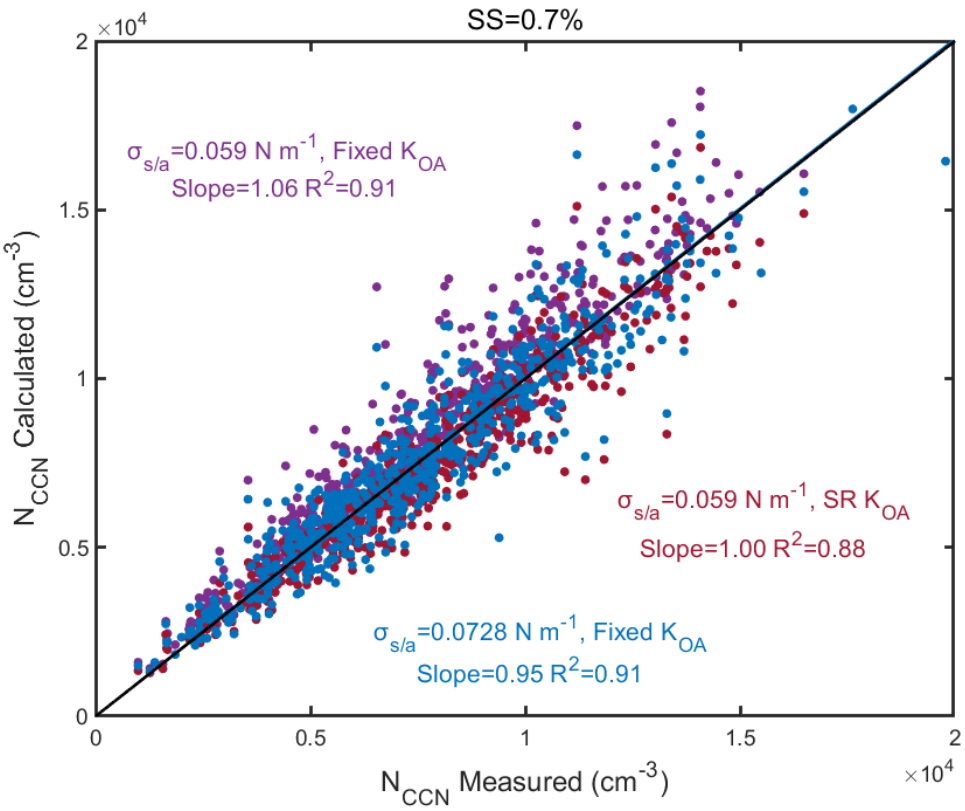

Figure S13. The predicted and measured N_{CCN} at 0.7% SS based on the $\sigma_{s/a}$ value (0.0728 N m^{-1}) for pure water and fixed κ_{OA} (blue dots), reduced $\sigma_{s/a}$ value (0.059 N m^{-1}) and fixed κ_{OA} (purple dots), and reduced $\sigma_{s/a}$ value (0.059 N m^{-1}) and SR κ_{OA} (red dots).

Reference:

Cai, M., Tan, H., Chan, C. K., Qin, Y., Xu, H., Li, F., Schurman, M. I., Liu, L., and Zhao, J.: The size-resolved cloud condensation nuclei (CCN) activity and its prediction based on aerosol hygroscopicity and composition in the Pearl Delta River (PRD) region during wintertime 2014, Atmos. Chem. Phys., 18, 16419-16437, https://doi.org/10.5194/acp-18-16419-2018, 2018.

Hong, J., Äijälä, M., Häme, S. A. K., Hao, L., Duplissy, J., Heikkinen, L. M., Nie, W., Mikkilä, J., Kulmala, M., Prisle, N. L., Virtanen, A., Ehn, M., Paasonen, P., Worsnop, D. R., Riipinen, I., Petäjä, T., and Kerminen, V. M.: Estimates of the organic aerosol volatility in a boreal forest using two independent methods, Atmos. Chem. Phys., 17, 4387-4399, https://doi.org/10.5194/acp-17-4387-2017, 2017.

Wang, J., Cubison, M., Aiken, A., Jimenez, J., and Collins, D.: The importance of aerosol mixing state and size-resolved composition on CCN concentration and the variation of the importance with atmospheric aging of aerosols, Atmos. Chem. Phys., 10, 7267-7283 , https://doi.org/10.5194/acp-10-7267-2010, 2010.